frontiers in Earth Science

ORIGINAL RESEARCH
published: 28 July 2020
doi: 10.3389/feart.2020.00261

Atmospheric Rivers Contribution to the Snow Accumulation Over the Southern Andes (26.5° S–37.5° S)

Felipe Saavedra[1], Gonzalo Cortés[2], Maximiliano Viale[3], Steven Margulis[4] and James McPhee[1,5]*

[1] Advanced Mining Technology Center, Universidad de Chile, Santiago, Chile, [2] Cetaqua, Centro Tecnológico del Agua, Santiago, Chile, [3] Instituto Argentino de Nivología, Glaciología y Ciencias Ambientales (IANIGLA) – Consejo Nacional de Investigaciones Científicas y Técnicas (CONICET), Mendoza, Argentina, [4] Civil and Environmental Engineering Department, University of California, Los Angeles, Los Angeles, CA, United States, [5] Departamento de Ingenieria Civil, Universidad de Chile, Santiago, Chile

This paper quantifies the climatological contribution of atmospheric rivers (ARs) to annual snow accumulation in the Andes Cordillera between 26.5° S and 36.5° S. An AR identification algorithm, and a high-resolution (0.01°) snow reanalysis dataset, both especially developed for this mountainous region, are used for this quantification over the 1984–2014 period. Results show that AR snowfall events explain approximately 50% of the annual snow accumulation over the study area, and are 2.5 times more intense than non-AR snowfall events. Due to orographic precipitation enhancement on the western slopes and a prominent rain shadow effect on the eastern slopes, annual snow accumulation and AR storms contribution to this accumulation are, on average, 7 and 12 times larger on western than on eastern slopes of the mountain range, respectively. Areas with lower peak elevations see more spillover snowfall over the eastern slopes of the mountain range, especially south of 35° S. Analysis of teleconnections with El Niño Southern Oscillation shows a reduction in the AR frequency across the study area during La Niña episodes and, consequently, a lower contribution to snow accumulation. Conversely, weak and moderate El Niño episodes show an increase in AR frequency, and consequently more snowfall.

Keywords: atmospheric rivers, Andes Cordillera, snow accumulation, ENSO, El Niño, rain shadow, South America

OPEN ACCESS

Edited by:
Bryan G. Mark,
The Ohio State University,
United States

Reviewed by:
Ulf Mallast,
Helmholtz Centre for Environmental Research (UFZ), Germany
Wei Zhang,
University of Iowa, United States

****Correspondence:***
Felipe Saavedra
fesaaved@uchile.cl

Specialty section:
This article was submitted to Hydrosphere, a section of the journal Frontiers in Earth Science

Received: *02 September 2019*
Accepted: *10 April 2020*
Published: *28 July 2020*

Citation:
Saavedra F, Cortés G, Viale M, Margulis S and McPhee J (2020) Atmospheric Rivers Contribution to the Snow Accumulation Over the Southern Andes (26.5° S–37.5° S). Front. Earth Sci. 8:261. doi: 10.3389/feart.2020.00261

1. INTRODUCTION

Snowmelt in the subtropical Andes Cordillera (25°–38° S) is the primary source of surface runoff during spring and summer months, having important implications for water supply and the local economy. Since 1970, an increase in the snow line elevation can be observed in this region, with a consequent decrease on average snow-covered area (Casassa et al., 2003; Carrasco et al., 2005). Since 2010, an unprecedented sequence of winter accumulation deficits has been observed, in what has come to be known as the Andean megadrought period (CR2, 2015; Boisier et al., 2016; Garreaud et al., 2019), this drought persists at the time of writing.

The accumulation of snow on the mid-latitudes Andes is usually produced by cold frontal systems originating in the Pacific Ocean, mostly during winter (Escobar and Aceituno, 1998). When cold fronts make landfall, the orographic effect of the Andes strongly enhance and reduce precipitation over the western and eastern side of the continental divide, respectively (e.g., Falvey and Garreaud, 2007; Viale et al., 2013). In addition, the strongest snowfall events are usually related

to intense water vapor transport from the Pacific Ocean in the pre-cold-front environment of cold frontal systems, which take the form of atmospheric rivers (ARs) (Viale and Nuñez, 2011).

ARs are narrow and elongated streams of intense water vapor that play an important role in the global water cycle and the local hydroclimate. In fact, they account for 84–88% of the total meridional Integrated Vapor Transport (IVT), covering 10% of Earth's circumference at midlatitudes (Zhu and Newell, 1998; Guan and Waliser, 2015). In California and western Europe, a contribution of 20–50% to annual precipitation and runoff has been estimated (e.g., Dettinger et al., 2011; Lavers and Villarini, 2015). Moreover, ARs are responsible for floods, extreme winds and related damages over the western U.S. and Europe (Ralph et al., 2006; Leung and Qian, 2009; Dettinger et al., 2011; Lavers et al., 2011, 2012; Neiman et al., 2011, 2013). Dettinger (2013) reports that ARs may also play a critical role in ending drought events on the coast of the Western United States.

On the west coast of South America, recent work by Viale et al. (2018) introduced a climatology of landfalling ARs and evaluated their impacts on precipitation. Landfalling ARs are most frequent between 38° and 50° S, averaging 35–40 AR days/year, and decrease rapidly to the north with just 10 AR days/year at 31° S. AR contributions to annual precipitation in subtropical Chile (32° S–38° S) is estimated to be 50%-65%, and median daily and hourly AR-related precipitation is 2–3 times larger than that of other storms. North of 32° S, the contribution reduces to <8% on the western side (Pacific-draining) of the Andes, while on the eastern side of the Andes ARs are infrequent, contributing less than 15% to annual precipitation.

Interannual variation of Precipitation in Central Chile is strongly influenced by El Niño Southern Oscillation (ENSO) phases, where more extreme precipitation events occur during El Niño (warm) and fewer during La Niña (cold) conditions (Escobar and Aceituno, 1998; Montecinos and Aceituno, 2003; Grimm and Tedeschi, 2009; Quintana and Aceituno, 2012). ENSO is also an important driving mechanism of year to year variations in snowpack accumulation (Rutllant and Fuenzalida, 1991; Escobar and Aceituno, 1998; Masiokas et al., 2010), and explains 25% of peak Snow Water Equivalent (SWE) variability (Cortés et al., 2016) with significant correlations between peak SWE and ENSO only in El Niño phase (Cortés and Margulis, 2017). In the western US coast, AR precipitation is modulated by ENSO, Madden-Julian Oscillation (MJO), Arctic Oscillation (AO), and Pacific/North American (PNA) teleconnections. In addition, combinations of MJO and the quasi-biennial oscillation (QBO) provide sub-seasonal predictive skill for anomalous AR activity in the west coast of North America (Guan and Waliser, 2015; Baggett et al., 2017; Mundhenk et al., 2018)

Past studies have suggested a considerable contribution of ARs to the snowpack in mountain regions. For example, over the Sierra Nevada, California Guan et al. (2013) reported that the high volume of snowpack accumulated during the 2010/2011 winter season was related to a positive anomaly in the number of AR snow events during that season. In addition, AR snow events contributed to 30–40% of the annual SWE accumulation in most years for that region, with that fraction determined in many cases by just one or two extreme events (Guan et al., 2010). In Antarctica, four and five ARs reaching the coastal Dronning Maud Land contributed 74–80% of the outstanding ice sheet surface mass balance during 2009 and 2011 (Gorodetskaya et al., 2014). By using only six snow measurement sites in the central Andes (30° S–35° S), Viale et al. (2018) reported that ARs contribute between 43 and 55% of observed snow accumulation between 2001 and 2015. However, the influence of ARs on snowpack spatiotemporal patterns over the full extent of the subtropical Andes is still largely unknown.

In this paper, a high-resolution snow reanalysis data set for the Andes is analyzed in conjunction with an AR catalog to determine the contribution of ARs to snow accumulation. In light of scarce snow measurements across the study domain, the use of a snow reanalysis provides an opportunity for improving our understanding of the influence of AR on the spatial patterns of snow accumulation. Given the important effect of ENSO on snowpack accumulation (Cortés and Margulis, 2017), the effects of AR events on the spatiotemporal variability of SWE during different ENSO phases are also analyzed.

2. GEOGRAPHICAL SETTING, DATA, AND METHODS

2.1. Geographic and Climatic Setting

Our study domain extends from 26.5° S to 37.5° S, and from 72° W to 68° W, spanning the subtropical Andes region and including the headwaters of 24 watersheds in Chile and Argentina (**Figure 1A**). These mountain catchments supply water for highly populated cities and important agricultural and industrial areas in both countries. **Figures 1B,C** show that snow accumulation on the western slopes is quite larger than on the eastern slopes of the subtropical Andes, and that most of the snow falls in winter as midlatitudes storm-tracks and AR storms migrate toward the equator (e.g., Hoskins and Hodges, 2005; Falvey and Garreaud, 2007). The crest of the Andes varies largely from 2,300 to 5,300 m.a.s.l. from 37.5° S to 26.5° S, which imply variations in cross-barrier orographic effects on precipitation. To the east of the crest, precipitation amounts are considerably reduced due to the rain shadow effect, which is greater between 32° and 34.5° S than between 35° and 36.5° S, probably due to lower crest altitude (Viale and Nuñez, 2011). To the west of the continental divide, annual precipitation increases from the Pacific coast to the western slopes by a factor of 1.8 ± 0.3 (Viale and Garreaud, 2015). In along-barrier direction, there is also a climatic gradient on the western side of the Andes, going from arid conditions (300–400 mm) at 26.5° S to more humid conditions (∼1,000–1,500 mm) at 37.5° S due to more baroclinic activity (e.g., Boisier et al., 2018).

2.2. AR and Snow Reanalysis Data

The occurrence of ARs landfall on western South America was obtained from an AR catalog derived from an AR detection algorithm for the South American region. This algorithm was developed by Viale et al. (2018) and uses the Integrated Vapor Transport variable from the Climate Forecast System Reanalysis (CFSR, Saha et al., 2010) gridded dataset. The CFSR grid has an 0.5° horizontal resolution, a temporal span from 1979 to present every 6-h timestep, and uses a coupled ocean–atmosphere–land

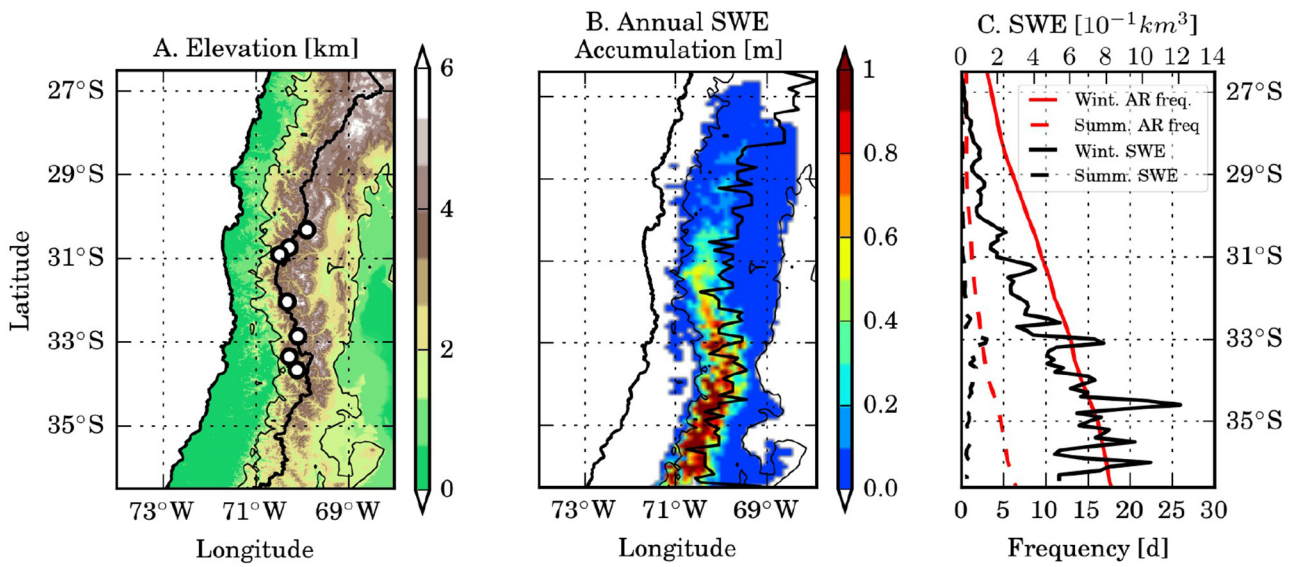

FIGURE 1 | (A) Topographic map of the Subtropical Andes. Surface snow measurement sites are indicated by white circles and the thick black lines indicate the border between Argentina and Chile and the coastline, while the thin black line indicate the 2,000 m elevation for reference. **(B)** Climatology of the Snow Water Equivalent (SWE) derived from the snow reanalysis over the 1984–2014 period [adapted from Cortés and Margulis (2017)]. Black thick lines show the coast line and the crest of Andes (maximum altitudes in snow reanalysis dataset); the 2,000 m elevation line is also indicated. **(C)** Variations with latitude of the Atmospheric River frequency along the Pacific coast (red lines) and of the areal mean SWE (black lines) for winter (Apr-Sep) and summer (Oct-Mar) seasons (continuous and dashed lines, respectively).

model to assimilate observations. Although the AR identification algorithm is described in detail in Viale et al. (2018), a brief explanation is given here. The algorithm follows as close as possible the definition of an AR which appeared in 2017 in the glossary of meteorology of the American Meteorological Society (AMS, Ralph et al., 2019). This is essentially a long and narrow corridor of intense water vapor transport usually associated with a midlatitude cold front. The algorithm detects a long and narrow corridor of intense IVT as an AR when its IVT values are greater than the 85th monthly percentile values in each grid cell, its length is larger than 2,000 km and its earth surface area to length ratio is greater than 2 (i.e., a metric for its width). Finally, the corridor must be associated with a near-surface frontal zone following the procedure proposed by Jenkner et al. (2010). We computed AR frequency as the number of AR time steps for a given period.

The Andean SWE Reanalysis (ASR) dataset developed by Cortés and Margulis (2017) and Cortés et al. (2014) was employed to analyze SWE variations. The dataset is generated using a particle batch smoother assimilation framework (Margulis et al., 2015). The land surface model (LSM) SSiB3 and a depletion curve model (DCM) were used to obtain prior estimates of SWE and fractional snow covered area (fSCA) respectively. Posteriorly fSCA values obtained from a Landsat imagery were assimilated to improve SWE estimations. Further details in the ASR development can be consulted in Margulis et al. (2016) and Cortés et al. (2016).

The ASR has daily data from April 1984 to March 2015 with a 0.001° spatial resolution. We aggregated SWE to a 0.1° resolution by the simple average for all analyzes. We estimate yearly peak SWE values as the maximum annual SWE value per pixel, in order to calculate annual correlations with AR frequency. In addition, we use maximum SWE annual values from 7 snow pillows from the Chilean national water agency (DGA, **Figure 1A**) to compute annual correlations with AR frequency. Daily accumulation from the SWE reanalysis was calculated by subtracting the SWE values of the previous day for each cell, keeping only positive values. This assumption neglects the effects of daily snow gravitational and wind transport between pixels.

2.3. AR Attribution to Snowpack Variations

Daily snow amount variations derived from the SWE reanalysis data was related to the presence of an AR by using the AR catalog. Since both products have different grid spacings and time steps, the AR catalog with coarser grid spacing (0.5°) was refined using a nearest neighbor interpolation to the 0.1° grid spacing of the SWE product.

By comparing both AR and SWE datasets with the same grid spacing and time period (1984-2014), a snowfall day was counted as AR-related when AR conditions were present at any grid cell on any of the four 6-h time steps that day. Then, if this criterion was met in 1 day, the snowfall in the day before and after were also related to the AR, in order to account for lead- and lag-time response between AR conditions and snowfall. A similar methodology was also used by Guan et al. (2010), Viale et al. (2018), and Huning et al. (2017, 2019). Additionally, high resolution (0.1°) topographic data from USGS was used

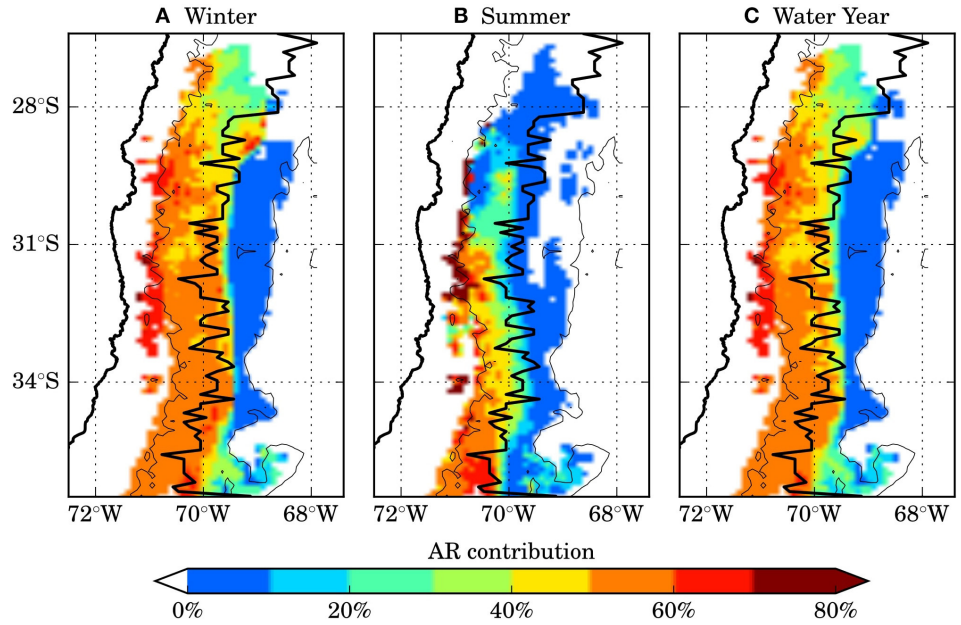

FIGURE 2 | Percentage AR contribution to **(A)** winter (Apr-Sep), **(B)** summer (Oct-Mar), and **(C)** annual total snow accumulation over the Subtropical Andes during the 1984–2014 period. Thick black lines show the crest of Andes and the coast line, while thin lines show the 2,000 m elevation for reference.

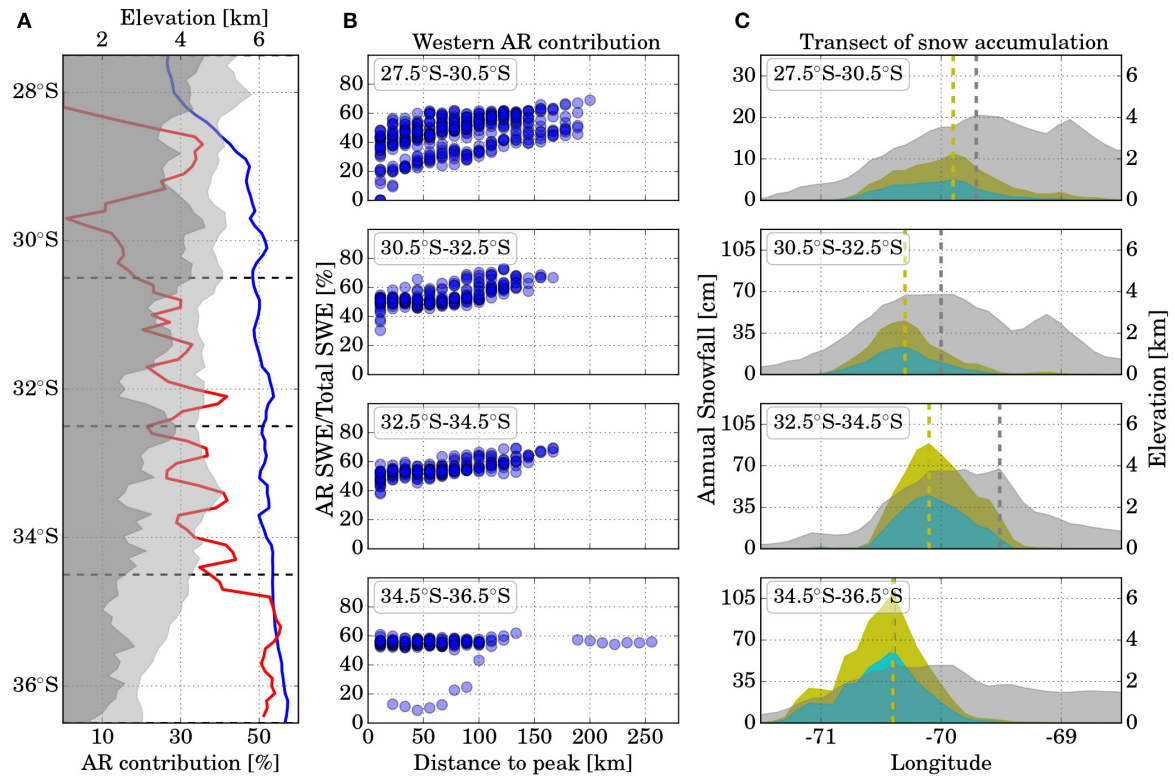

FIGURE 3 | (A) Variations with latitude (i.e., along-barrier direction) of the crestline (light gray), of the topographic altitude 40 km to the west (upwind) of the crest of the Andes (dark gray), and of the AR contribution to the annual snow accumulation on the western (blue line) and eastern (red line) slopes, respectively. Transects showing the variations in cross-barrier direction of **(B)** the AR contribution on pixel scales over the western (blue circles), and **(C)** the annual total (yellow) and AR-related (green) annual snow accumulation. The meridionally-averaged peak of the snow accumulation and of the maximum topographic elevation (crest) are shown as dotted yellow and gray lines, respectively.

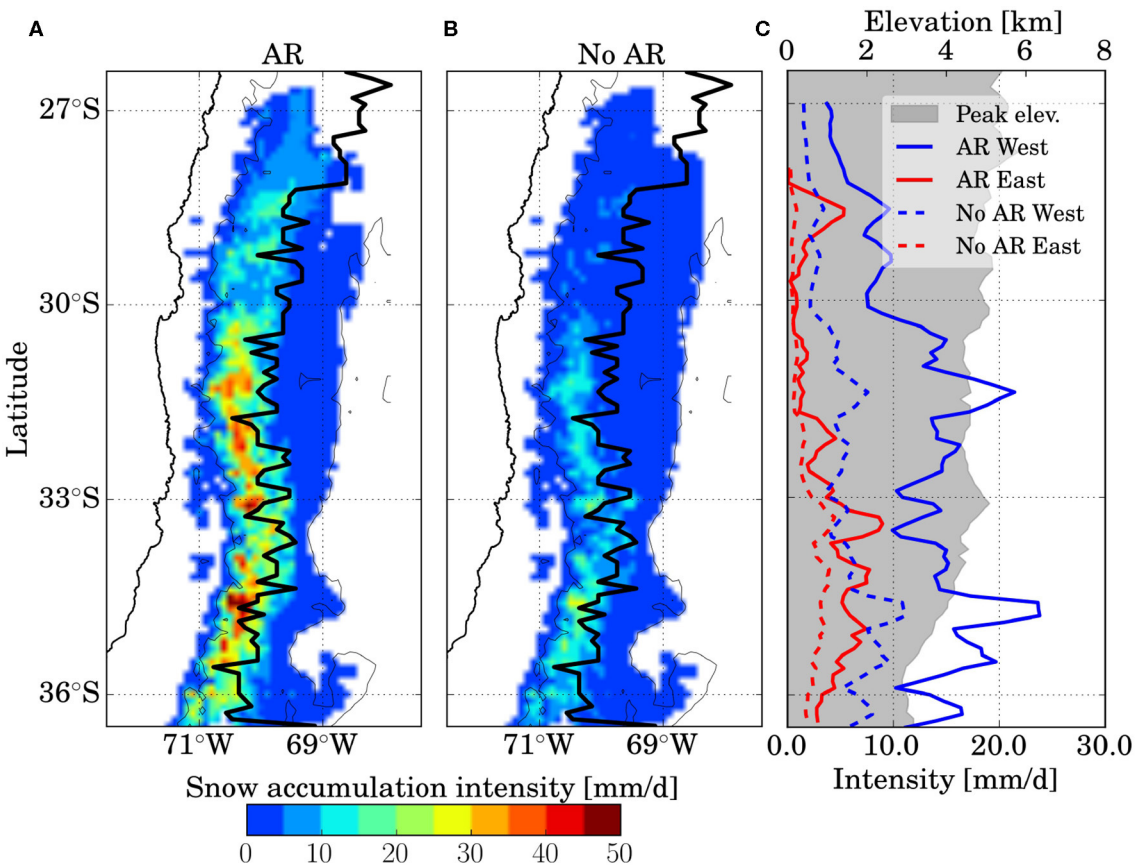

FIGURE 4 | Mean daily snowfall intensity for **(A)** the AR and **(B)** the non-AR snowfall events on pixel scales. The crest of the Andes and the 2,000 m topographic line are plotted by thick and thin black lines, respectively. **(C)** Variations with latitude of the altitude of the crestline (shaded in gray) and of the mean daily snowfall intensity on the western (blue lines) and eastern (red lines) slopes for the AR (continuous lines) and non-AR (dashed lines) snowfall event.

to determine the crest of the Andes chain at different latitudes in order to compare AR influences on snow over western and eastern slopes of the Andes.

The ENSO correlation with SWE and AR frequency is explored to understand variability in AR contribution. ENSO teleconnections were analyzed by classifying years based on the Oceanic Niño Index (ONI). An ENSO phase (El Niño or La Niña) is defined when a minimum of five consecutive overlapping months are above/below ±0.5°C, following NOAA Climate Prediction methodology (http://www.cpc.ncep.noaa.gov). In this study, we use an arbitrary classification scheme from Cortés and Margulis (2017), in order to further define the year categorization. Taking into account the months between April and October (including AMJ, MJJ, JJA, and JAS values), we define a Moderate to Strong El Niño (MSE) if the ENSO 3.4 anomaly value is over 1°C; a Weak El Niño (WE) if ENSO 3.4 is between 0.5 and 1°C; a Weak La Niña (WL) if ENSO 3.4 is between −0.5 and −1°C; and Moderate to Strong La Niña (MSL) for ENSO 3.4 values lower than −1°C. This classification yields 4 MSL, 7 WL, 4 WE, and 3 MSE years within the study period.

3. RESULTS

3.1. ARs Contribution to Snowpacks

Coherent with climatic conditions described above, ARs make landfall on the subtropical west coast of South America mostly during winter, and increases from <10 AR days at 26.5° S to 30 AR days at 37.5° S annually (see also Figure 7 of Viale et al., 2018). Despite the large spatial variation of snow accumulation in the study domain, the overall contribution of ARs to the annual total snow accumulation on the western and immediate eastern sides of the crest of the Andes is estimated to be 51% (**Figure 2C**). Farther east of the crest, the snowfall drops drastically down to near zero values due to a prominent rain shadow effect, and so does the AR contribution. AR contribution to snow accumulation is greater in the wet, winter season (53%) than in the dry, summer season (<30%), further highlighting the great importance of ARs in supplying water in the region (c.f, **Figures 2A,B**). Although the snow accumulation maximum is observed on the high western slopes close to the crest, both seasonal and annual total AR contribution plots of **Figure 2** show that the AR contribution is slightly larger on lower western (windward) slopes than on high terrain close to the crest. This

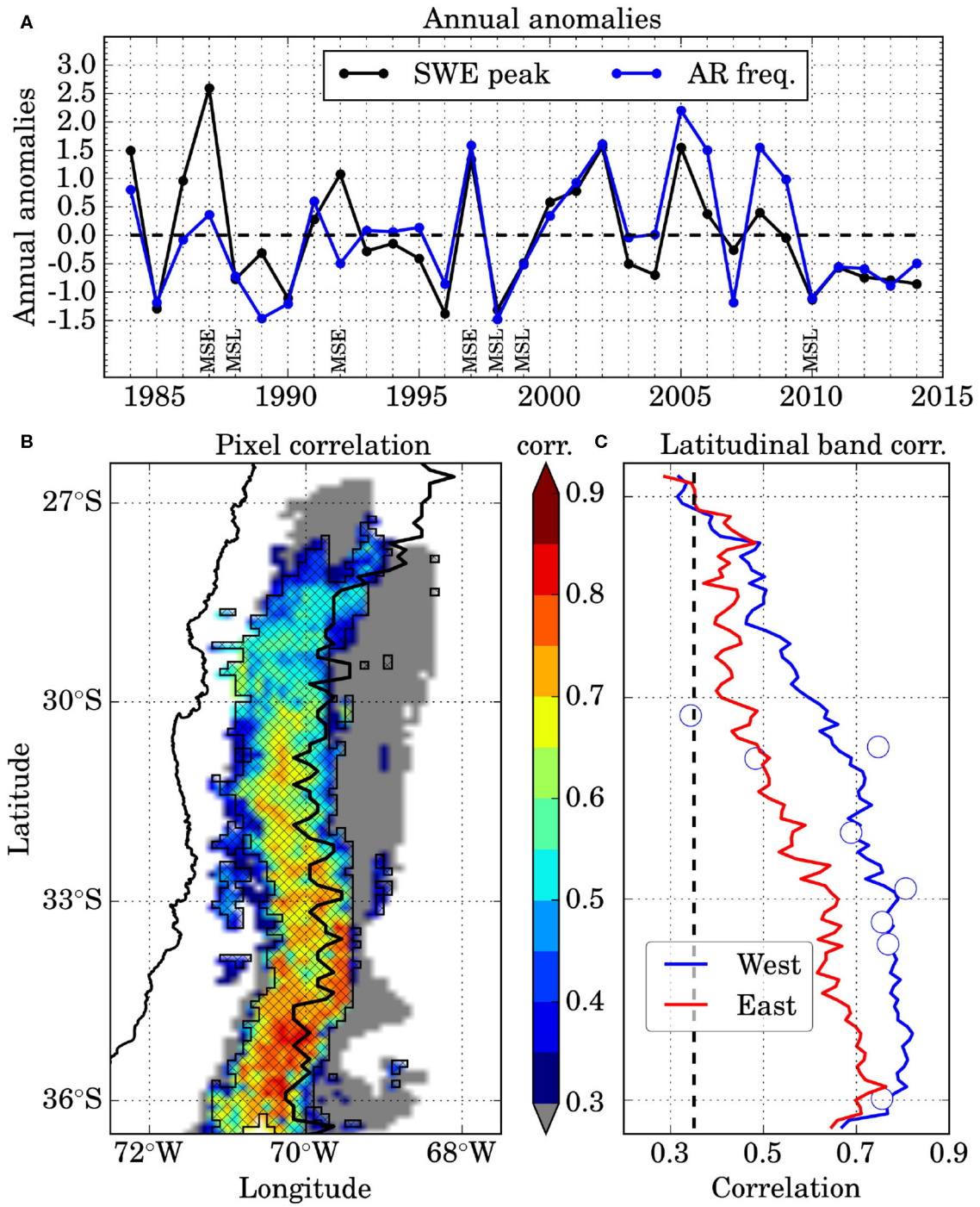

FIGURE 5 | (A) Time series of annual standardized anomalies of the regional SWE peak and AR contribution to snow accumulation. **(B)** Correlation between annual time series of peak SWE peak and AR frequency on the pixel scale (dashed pixels indicate significant correlation). Thick black line indicates the crest of the Andes. **(C)** Variation with latitude of correlations between annual time series of SWE peak and AR frequency latitudinally averaged on the western (blue) and eastern (red) slopes. The correlations at some available Snow pillows sites are shown by the circles. Dashed black lines represent the 95% significance level for the correlations.

feature is further demonstrated in transects of **Figure 3C**, and could be a response of greater orographic enhancement of precipitation on the first rise of the strong, cross-barrier moisture flux from ARs as has been suggested by other studies on the coastal western mountains of North America (Neiman et al., 2017; Zagrodnik et al., 2018, 2019).

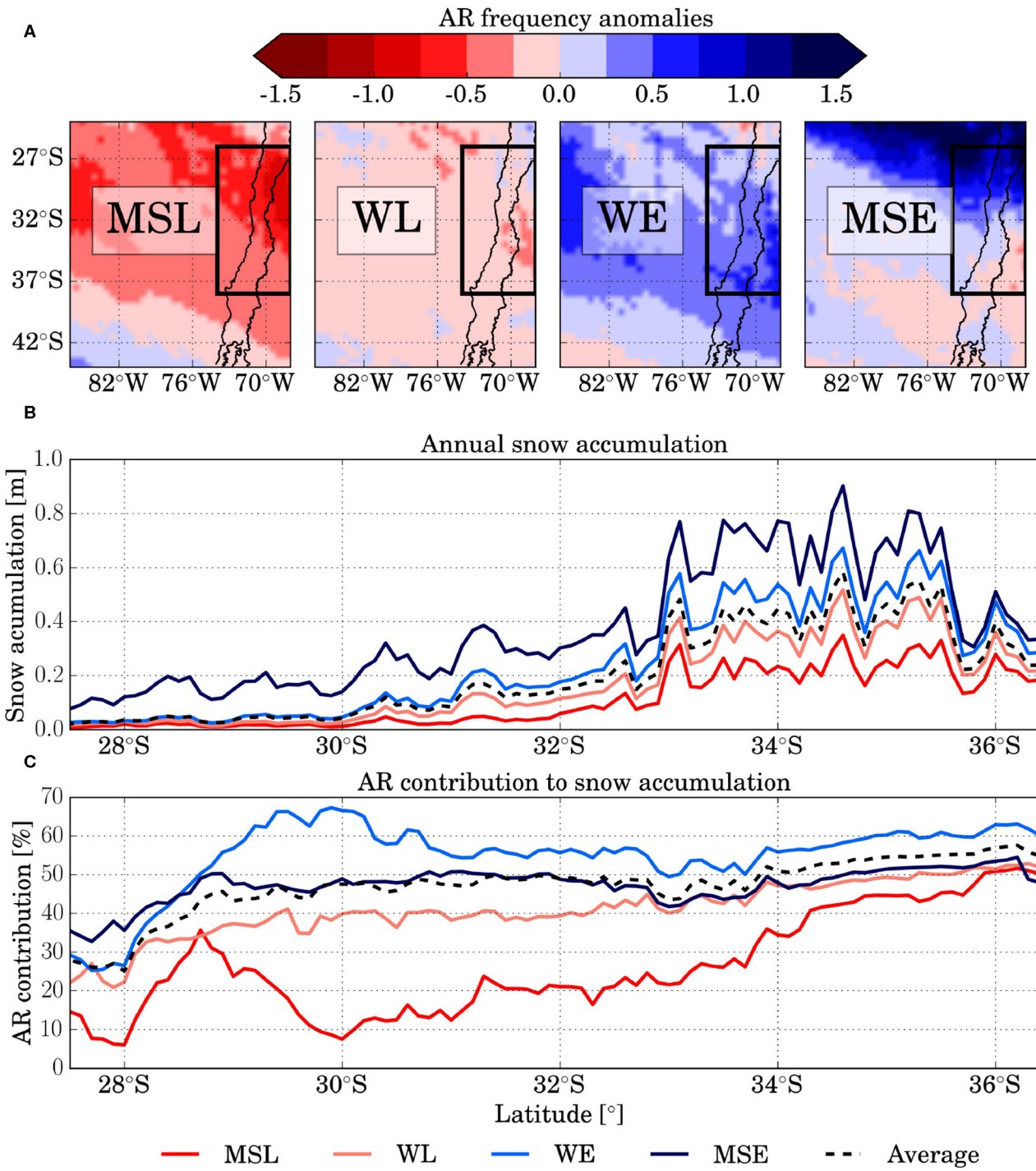

FIGURE 6 | (A) Standardized anomalies of AR frequency for different ENSO phases: moderate to strong La Niña (MSL), weak La Niña (WL), weak El Niño (WE) and moderate to strong El Niño (MSE). The black rectangles delimit the study zone and black lines show coastline and political border between Chile and Argentina. **(B)** Variation with latitude of latitudinally-averaged snow accumulation for the different ENSO phases and average year. **(C)** Same as **(B)** but for AR contribution to the annual snow accumulation.

Figure 3 illustrates the strong orographic effects of the Andes on the snow accumulation and the ARs contribution to this accumulation in along- and cross-barrier directions. While the AR contribution on the western slopes varies gradually from 30% at 27.5° S to 60% at 36.5° S, the AR contribution on the eastern slopes alternates between sectors with 0x and 50% of contribution

(**Figure 3A**). This variation seems to follow closely changes in the Andes height. North of 34° S, where the mountain range is higher (>4,000 m), areas with near zero contribution correspond to high peaks (>5,000 m) where westerly moisture transporting airflow are unable overpass to the lee; areas with increased contribution correspond to low valleys or passageways where westerly airflow is able to overpass. South of 34° S where the Andes are lower on average (<4,000 m), the highest contribution on eastern slopes are observed (50%) being similar to those on the western slopes (**Figure 3A**) and almost never reaching such low values as on the northern subdomain. Cross-barrier plots in **Figure 3C** highlight the large difference in snow accumulation between both sides of the Andes, which is about 2–15 times larger (7 on average) on the western than on the eastern slopes for the different subdomains and for AR storms it is about 1.5–40 times larger (12 on average). The transects also show how the maximum in accumulation occurs farther upstream from the crest of the Andes as the height of the crest increases (c.f, **Figures 3A–D**). While the maximum snow accumulation occurs close to the crest of the Andes between 35 and 37° S, this maximum occurs between 50 km and 100 km upstream of the crest north of 35° S. This result is in line with previous studies documenting orographic precipitation pattern in other mountain ranges (e.g., Roe, 2005), and responds to the physical Clausius-Clapeyron phenomenon, which explains how the holding capacity of water vapor drops abruptly with temperature. In other words, as temperature decreases strongly with altitude, the capacity of the atmosphere to hold unsaturated water vapor reduces abruptly, and so the amount of condensate and freezing liquid water (snow) on higher western slopes.

In order to evaluate the snowfall intensity under AR conditions, mean daily snow accumulation per pixel was computed using days with $\Delta SWE>0$ for AR and non-AR events (**Figure 4**). Domain-averaged snowfall intensity during AR events is 8.1 mm/day, which is 2.5 times more intense than snowfall intensity during non-AR events (3.2 mm/day). The highest snowfall intensities are observed upwind of the crest and south of 31° S during AR storms (**Figure 4A**). On both sides of the crest, there is an increase in snowfall intensity during AR storms compared with non-AR storms, although the overall snowfall intensities are quite lower on the eastern than on the western slopes regardless of the presence of AR.

3.2. Interannual Variability and ENSO Teleconnections

The interannual variability of snowpacks in the subtropical Andes and their connections with AR frequency and the ENSO phenomenon are explored in this section. To this end, the correlation between SWE and AR frequency is analyzed in **Figure 5**. In particular, at the regional scale, the correlation between the anomalies of the annual peak SWE areal average and AR frequency is high (0.73) and significative (**Figure 5A**), suggesting a strong dependence of the annual peak SWE on AR occurrence over this region of the Andes. Consistent with the previous analysis, the spatial correlation between annual peak SWE and AR frequency at the pixel scale shows higher (significative) correlation values on the western than on the eastern slopes of the Andes (**Figures 5B,C**), ranging from 0.9 to less than 0.3, respectively. These results denote a stronger dependence of annual snow accumulation on AR occurrence toward the southern sector and on the western (windward side) slopes. Interestingly, the estimated highest values of AR contribution on the lower western slopes (**Figure 2**) do not correspond with high values in correlation, which may be explained by the relatively low altitude of this sector on the foothills, where an alternation between liquid and solid precipitation depending on temperature may be frequent. This phenomenon may degrade the correlation as the few AR snowfall events contribute largely to the annual total snow.

The connection between the different ENSO phases, AR frequency, and snow accumulation is analyzed in **Figure 6**. During the warm (cold) phase AR landfalls frequency in the central Chilean coast increase (decrease) (**Figure 6A**). This behavior is consistent with some previous results. For example, Montecinos and Aceituno (2003) documented wet (dry) conditions in central Chile (30°–35° S) during the warm (cold) phase of ENSO associated with an equatorward (poleward) displacement of wintertime storm track (e.g., Karoly, 1989; Seager et al., 2005). This ENSO-related pattern has a resemblance to those documented by Zhang and Villarini (2018) in the North Pacific, which also produce more AR activity and precipitation in the southwest of the US, a region with climatic features very similar to those in central Chile. More recently, Guan and Waliser (2015) reported an increase (decrease) of AR frequency in our study area under El Niño (La Niña) conditions and linked this pattern to an anomaly in the South Pacific Convergence Zone (SPCZ). For the warm (cold) phase of ENSO, it has been also reported a northeastward (southwestward) shift of the SPCZ as a result of ENSO derived meridional sea surface temperature gradients variations (Folland et al., 2002; Widlansky et al., 2013; Sulca et al., 2018).

Large absolute differences in snow accumulation can be seen across the study area during Moderate to Strong el Niño (MSE) conditions, with a stronger effect on the northern subdomain. Conversely, AR contribution is higher during Weak El Niño (WE) conditions, particularly between 29° and 31° S, indicating an "optimum" in which for warmer ENSO 3.4 conditions, other precipitation-originating fronts take relevance as moisture sources. Conversely, for cold anomaly conditions (La Niña), AR contribution decreases sharply north of 34° S. This result is in strong agreement with previous findings, which point at a sharp precipitation gradient located approximately at 34° S (Aravena and Luckman, 2009; González-Reyes et al., 2017). A more consistent regime of AR south of this latitude is likely to explain this transition.

4. CONCLUSIONS

The contribution of ARs to the snow accumulation in the southern Andes (27.5°–37.5° S) has been quantified in this study by using an AR catalog and a snow reanalysis dataset both specifically developed for this South American region. Results show that AR events play an important role in snow

accumulation, contributing, on average, 51% of annual total snow accumulation across the entire study area. This estimation is similar to those (43–55%) provided by Viale et al. (2018) based on a few snow pillows located between 30° S and 36° S, and are also comparable with those obtained for the Sierra Nevada by Huning et al. (2017, 2019), who estimate 52–62% using a similar methodology, whereas Guan et al. (2013) found a lower contribution of 37%.

In this study, AR snowfall events are shown to be 2.5 times more intense than non-AR snowfall events, in agreement with previous results in other mountain ranges, such as the Sierra Nevada and the Cascades in US (Neiman et al., 2008; Guan et al., 2010), and in the same Andean region (Viale et al., 2018). Due to the strong orographic effects of the Andes on precipitation, the snow accumulation and the AR storms contribution to this accumulation is, on average, 7 and 12 times larger on the western than on the eastern slopes, respectively. The basic physical mechanism that explains this main result is the orographic ascend and descend of the large-scale westerly airflow associated with snowstorms that follow the shape of the barrier, and favored an orographic precipitation enhancement and reduction of snow on the western and eastern slopes of the Andes, respectively. Some variations with latitude in this orographic effects are observed caused by variations in the height of the Andes, especially south of 35° S where they are lower and more spillover snowfall is observed on the eastern slopes. Unlike the few snow measurement sites available in the Andes, the snow reanalysis dataset has allowed this detailed description of snow distribution and the role of ARs on it over the entire Andes range. Overall, our findings are coherent with orographic precipitation patterns observed on other mountain ranges [e.g., see the review of Roe (2005)].

AR activity and snow accumulation show large interannual variability in the study region. We found significant positive correlations between peak SWE and AR activity, showing the potential of estimating peak SWE based on AR data. Interannual SWE variability is found to be modulated by ENSO in agreement with previous studies (e.g., Cortés and Margulis, 2017). During La Niña episodes there is a decrease in AR activity and a smaller AR influence in snow accumulation. El Niño phase is known to promote more snowfall. For weak El Niño episodes AR activity and their snow contribution increase in the entire study area. However, we find that moderate to strong El Niño episodes displace AR landfall northward reducing the partial contribution south of 32° S. This can be explained due to the equatorward shift of the wintertime storm tracks during ENSO warm phase and bears a resemblance with ENSO-related patterns founded in northern Pacific.

The findings of this study agree with previous research that shows midlatitude frontal systems to be connected with atmospheric rivers encountering mountainous coastal terrains, such as the west coast of North America and Europa. These storms are well-known to potentially produce heavy orographic precipitation and provide a large fraction of water resources. Previous results in the Andes have confirmed these findings using only a few snow sites and our results here have moved forward by using a high-resolution snow dataset that covers the entire mountain range. This paper expands the understanding of the AR contribution to snow and water supply over different sectors of the Andes, such as their contribution on the first rise or different eastern and western slopes of the range, which may be useful for water management agencies in both countries, Chile and Argentina. In addition, new knowledge about the relationship between the AR storms and the large-scale ENSO phenomena, which is one of the main drivers of interannual snow accumulation, is provided here. For a whole understanding of the ARs in the modulation of snapbacks on this sector of the Andes, future works may deal with the role of AR in relation to rain-on-snow events, which has been proven to be significant in other mountain ranges.

DATA AVAILABILITY STATEMENT

The datasets generated for this study are available on request to the corresponding author.

AUTHOR CONTRIBUTIONS

All authors contributed conception and design of the study. GC and MV provided and organized source data. All authors contributed to manuscript writing, revision, read, and approved the submitted version.

FUNDING

This research was supported by CONICYT Project AFB180004 and FONDECYT Project 1171032. MV was supported by FONDECYT 11151009.

ACKNOWLEDGMENTS

Snow pillow data was obtained from Direccion General de Aguas (DGA) from Chile. We thank Pablo Mendoza, Thomas Shaw, and two reviewers for valuable contributions that have improved the original manuscript.

REFERENCES

Aravena, J.-C., and Luckman, B. H. (2009). Spatio-temporal rainfall patterns in Southern South America. *Int. J. Climatol.* 29, 2106–2120. doi: 10.1002/joc.1761

Baggett, C. F., Barnes, E. A., Maloney, E. D., and Mundhenk, B. D. (2017). Advancing atmospheric river forecasts into subseasonal-to-seasonal time scales. *Geophys. Res. Lett.* 44, 7528–7536. doi: 10.1002/2017GL074434

Boisier, J. P., Alvarez-Garretón, C., Cordero, R. R., Damiani, A., Gallardo, L., Garreaud, R. D., et al. (2018). Anthropogenic drying in central-southern Chile evidenced by long-term observations and climate model simulations. *Elem. Sci. Anth.* 6:74. doi: 10.1525/elementa.328

Boisier, J. P., Rondanelli, R., Garreaud, R. D., and Muñoz, F. (2016). Anthropogenic and natural contributions to the Southeast Pacific precipitation decline and recent megadrought in central Chile. *Geophys. Res. Lett.* 43, 413–421. doi: 10.1002/2015GL067265

Carrasco, J. F., Casassa, G., and Quintana, J. (2005). Changes of the 0°C isotherm and the equilibrium line altitude in central Chile during the last quarter of the 20th century / Changements de l'isotherme 0°C et de la ligne d'équilibre des neiges dans le Chili central durant le dernier quart du 20éme siécle. *Hydrol. Sci. J.* 50, 933–948. doi: 10.1623/hysj.2005.50.6.933

Casassa, G., Rivera, A., Escobar, F., Acuña, C., Carrasco, J., and Quintana, J. (2003). Snow line rise in central Chile in recent decades and its correlation with climate. *Geophys. Res. Abstr.* 5:14395.

Cortés, G., Girotto, M., and Margulis, S. (2016). Snow process estimation over the extratropical Andes using a data assimilation framework integrating MERRA data and Landsat imagery. *Water Resour. Res.* 52, 2582–2600. doi: 10.1002/2015WR018376

Cortés, G., Girotto, M., and Margulis, S. A. (2014). Analysis of sub-pixel snow and ice extent over the extratropical Andes using spectral unmixing of historical Landsat imagery. *Remote Sens. Environ.* 141, 64–78. doi: 10.1016/j.rse.2013.10.023

Cortés, G., and Margulis, S. (2017). Impacts of El Niño and La Niña on interannual snow accumulation in the Andes: results from a high-resolution 31 year reanalysis. *Geophys. Res. Lett.* 44, 6859–6867. doi: 10.1002/2017GL073826

CR2 (2015). *Report to the Nation. The 2010-2015 Mega-Drought: A Lesson for the Future*. Center for Climate and Resilience Research (CR2), 28.

Dettinger, M. D. (2013). Atmospheric rivers as drought busters on the U.S. West Coast. *J. Hydrometeorol.* 14, 1721–1732. doi: 10.1175/JHM-D-13-02.1

Dettinger, M. D., Ralph, F. M., Das, T., Neiman, P. J., and Cayan, D. R. (2011). Atmospheric rivers, floods and the water resources of California. *Water* 3, 445–478. doi: 10.3390/w3020445

Escobar, F., and Aceituno, P. (1998). Influencia del fenomeno ENSO sobre la precipitacion nival en el sector andino de Chile Central durante el invierno. *Mech. Ageing Dev.* 4, 201–213.

Falvey, M., and Garreaud, R. (2007). Wintertime precipitation episodes in central Chile: associated meteorological conditions and orographic influences. *J. Hydrometeorol.* 8, 171–193. doi: 10.1175/JHM562.1

Folland, C. K., Renwick, J. A., Salinger, M. J., and Mullan, A. B. (2002). Relative influences of the Interdecadal Pacific Oscillation and ENSO on the South Pacific Convergence Zone. *Geophys. Res. Lett.* 29, 21-1–21-4. doi: 10.1029/2001GL014201

Garreaud, R. D., Boisier, J. P., Rondanelli, R., Montecinos, A., Sepúlveda, H. H., and Veloso-Aguila, D. (2019). The Central Chile Mega Drought (2010-2018): A climate dynamics perspective. *Int. J. Climatol.* 40, 421–439. doi: 10.1002/joc.6219

González-Reyes, Á., McPhee, J., Christie, D. A., Quesne, C. L., Szejner, P., Masiokas, M. H., et al. (2017). Spatiotemporal variations in hydroclimate across the Mediterranean Andes (30°-37° S) since the early twentieth century. *J. Hydrometeorol.* 18, 1929–1942. doi: 10.1175/JHM-D-16-0004.1

Gorodetskaya, I. V., Tsukernik, M., Claes, K., Ralph, M. F., Neff, W. D., and Van Lipzig, N. P. M. (2014). The role of atmospheric rivers in anomalous snow accumulation in East Antarctica. *Geophys. Res. Lett.* 41, 6199–6206. doi: 10.1002/2014GL060881

Grimm, A. M., and Tedeschi, R. G. (2009). ENSO and extreme rainfall events in South America. *J. Clim.* 22, 1589–1609. doi: 10.1175/2008JCLI2429.1

Guan, B., Molotch, N. P., Waliser, D. E., Fetzer, E. J., and Neiman, P. J. (2010). Extreme snowfall events linked to atmospheric rivers and surface air temperature via satellite measurements. *Geophys. Res. Lett.* 37, 2–7. doi: 10.1029/2010GL044696

Guan, B., Molotch, N. P., Waliser, D. E., Fetzer, E. J., and Neiman, P. J. (2013). The 2010/2011 snow season in California's Sierra Nevada: role of atmospheric rivers and modes of large-scale variability. *Water Resour. Res.* 49, 6731–6743. doi: 10.1002/wrcr.20537

Guan, B., and Waliser, D. E. (2015). Detection of atmospheric rivers: Evaluation and application of an algorithm for global studies. *J. Geophys. Res. Atmos.* 120, 12514–12535. doi: 10.1002/2015JD024257

Hoskins, B. J., and Hodges, K. I. (2005). A new perspective on Southern Hemisphere storm tracks. *J. Clim.* 18, 4108–4129. doi: 10.1175/JCLI3570.1

Huning, L. S., Guan, B., Waliser, D. E., and Lettenmaier, D. P. (2019). Sensitivity of seasonal snowfall attribution to atmospheric rivers and their reanalysis-based detection. *Geophys. Res. Lett.* 46, 794–803. doi: 10.1029/2018GL080783

Huning, L. S., Margulis, S. A., Guan, B., Waliser, D. E., and Neiman, P. J. (2017). Implications of detection methods on characterizing atmospheric river contribution to seasonal snowfall across Sierra Nevada, USA. *Geophys. Res. Lett.* 44, 10445–10453. doi: 10.1002/2017GL075201

Jenkner, J., Sprenger, M., Schwenk, I., Schwierz, C., Dierer, S., and Leuenberger, D. (2010). Detection and climatology of fronts in a high-resolution model reanalysis over the Alps. *Meteorol. Appl.* 17, 1–18. doi: 10.1002/met.142

Karoly, D. J. (1989). Southern hemisphere circulation features associated with El Niño-southern oscillation events. *J. Clim.* 2, 1239–52. doi: 10.1175/1520-0442(1989)002h1239:SHCFAWi2.0.CO;2

Lavers, D. A., Allan, R. P., Wood, E. F., Villarini, G., Brayshaw, D. J., and Wade, A. J. (2011). Winter floods in Britain are connected to atmospheric rivers. *Geophys. Res. Lett.* 38, 1–8. doi: 10.1029/2011GL049783

Lavers, D. A., and Villarini, G. (2015). The contribution of atmospheric rivers to precipitation in Europe and the United States. *J. Hydrol.* 522, 382–390. doi: 10.1016/j.jhydrol.2014.12.010

Lavers, D. A., Villarini, G., Allan, R. P., Wood, E. F., and Wade, A. J. (2012). The detection of atmospheric rivers in atmospheric reanalyses and their links to British winter floods and the large-scale climatic circulation. *J. Geophys. Res. Atmos.* 117, 1–13. doi: 10.1029/2012JD018027

Leung, L. R., and Qian, Y. (2009). Atmospheric rivers induced heavy precipitation and flooding in the western U.S. simulated by the WRF regional climate model. *Geophys. Res. Lett.* 36:L03820. doi: 10.1029/2008GL036445

Margulis, S. A., Cortés, G., Girotto, M., and Durand, M. (2016). A landsat-era Sierra Nevada snow reanalysis (1985-2015). *J. Hydrometeorol.* 17, 1203–1221. doi: 10.1175/JHM-D-15-0177.1

Margulis, S. A., Girotto, M., Cortés, G., and Durand, M. (2015). A particle batch smoother approach to snow water equivalent estimation. *J. Hydrometeorol.* 16, 1752–1772. doi: 10.1175/JHM-D-14-0177.1

Masiokas, M. H., Villalba, R., Luckman, B. H., and Mauget, S. (2010). Intra- to multidecadal variations of snowpack and streamflow records in the Andes of Chile and Argentina between 30° and 37° S. *J. Hydrometeorol.* 11, 822–831. doi: 10.1175/2010JHM1191.1

Montecinos, A., and Aceituno, P. (2003). Seasonality of the ENSO-related rainfall variability in central Chile and associated circulation anomalies. *J. Clim.* 16, 281–296. doi: 10.1175/1520-0442(2003)016<0281:SOTERR>2.0.CO;2

Mundhenk, B. D., Barnes, E. A., Maloney, E. D., and Baggett, C. F. (2018). Skillful empirical subseasonal prediction of landfalling atmospheric river activity using the Madden-Julian oscillation and quasi-biennial oscillation. *NPJ Clim. Atmos. Sci.* 1:20177. doi: 10.1038/s41612-017-0008-2

Neiman, P. J., Gaggini, N., Fairall, C. W., Aikins, J., Spackman, J. R., Leung, L. R., et al. (2017). An analysis of coordinated observations from NOAA's Ronald H. Brown ship and G-IV aircraft in a landfalling atmospheric river over the North Pacific during CalWater-2015. *Mthly. Weather Rev.* 145, 3647–3669. doi: 10.1175/MWR-D-17-0055.1

Neiman, P. J., Ralph, F. M., Moore, B. J., Hughes, M., Mahoney, K. M., Cordeira, J. M., et al. (2013). The landfall and inland penetration of a flood-producing atmospheric river in Arizona. Part I: observed synoptic-scale, orographic, and hydrometeorological characteristics. *J. Hydrometeorol.* 14, 460–484. doi: 10.1175/JHM-D-12-0101.1

Neiman, P. J., Ralph, F. M., Wick, G. A., Lundquist, J. D., and Dettinger, M. D. (2008). Meteorological characteristics and overland precipitation impacts of atmospheric rivers affecting the West Coast of North America based on eight years of SSM/I satellite observations. *J. Hydrometeorol.* 9, 22–47. doi: 10.1175/2007JHM855.1

Neiman, P. J., Schick, L. J., Ralph, F. M., Hughes, M., and Wick, G. A. (2011). Flooding in Western Washington: the connection to atmospheric rivers*. *J. Hydrometeorol.* 12, 1337–1358. doi: 10.1175/2011JHM1358.1

Quintana, J. M., and Aceituno, P. (2012). Changes in the rainfall regime along the extratropical west coast of South America (Chile): 30-43º S. *Atmósfera* 25, 1–22. Available online at: http://www.scielo.org.mx/scielo.php?script=sci_arttext&pid=S0187-62362012000100001&lng=es&tlng=en

Ralph, F. M., Neiman, P. J., Wick, G. A., Gutman, S. I., Dettinger, M. D., Cayan, D. R., et al. (2006). Flooding on California's Russian River: Role of atmospheric rivers. *Geophys. Res. Lett.* 33:L13801. doi: 10.1029/2006GL026689

Ralph, F. M., Rutz, J. J., Cordeira, J. M., Dettinger, M., Anderson, M., Reynolds, D., et al. (2019). A scale to characterize the strength and impacts of atmospheric rivers. *Bull. Amer. Meteor. Soc.* 100, 269–289. doi: 10.1175/BAMS-D-18-0023.1

Roe, G. H. (2005). Orographic precipitation. *Annu. Rev. Earth Planet. Sci.* 33, 645–671. doi: 10.1146/annurev.earth.33.092203.122541

Rutllant, J., and Fuenzalida, H. (1991). Synoptic aspects of the central Chile rainfall variability associated with the Southern Oscillation. *Int. J. Climatol.* 11, 63–76. doi: 10.1002/joc.3370110105

Saha, S., Moorthi, S., Pan, H.-L., Wu, X., Wang, J., Nadiga, S., et al. (2010). The NCEP climate forecast system reanalysis. *Bull. Am. Meteorol. Soc.* 91, 1015–1058. doi: 10.1175/2010BAMS3001.1

Seager, R., Harnik, N., Robinson, W. A., Kushnir, Y., Ting, M., Huang, H.-P., et al. (2005). Mechanisms of ENSO-forcing of hemispherically symmetric precipitation variability. *Q. J. R. Meteorol. Soc.* 131, 1501–27. doi: 10.1256/qj.04.96

Sulca, J., Takahashi, K., Espinoza, J.-C., Vuille, M., and Lavado-Casimiro, W. (2018). Impacts of different ENSO flavors and tropical Pacific convection variability (ITCZ, SPCZ) on austral summer rainfall in South America, with a focus on Peru. *Int. J. Climatol.* 38, 420–435. doi: 10.1002/joc.5185

Viale, M., and Garreaud, R. (2015). Orographic effects of the subtropical and extratropical Andes on upwind precipitating clouds. *J. Geophys. Res. Atmos.* 120, 4962–74. doi: 10.1002/2014JD023014

Viale, M., Houze, R. A., and Rasmussen, K. L. (2013). Upstream orographic enhancement of a narrow cold-frontal rainband approaching the Andes. *Mthly. Weather Rev.* 141, 1708–1730. doi: 10.1175/MWR-D-12-00138.1

Viale, M., and Nuñez, M. N. (2011). Climatology of winter orographic precipitation over the subtropical central Andes and associated synoptic and regional characteristics. *J. Hydrometeorol.* 12, 481–507. doi: 10.1175/2010JHM1284.1

Viale, M., Valenzuela, R., Garreaud, R. D., and Ralph, F. M. (2018). Impacts of atmospheric rivers on precipitation in southern south America. *J. Hydrometeorol.* 19, 1671–1687. doi: 10.1175/JHM-D-18-0006.1

Widlansky, M. J., Timmermann, A., Stein, K., McGregor, S., Schneider, N., England, M. H., et al. (2013). Changes in South Pacific rainfall bands in a warming climate. *Nat. Clim. Change* 3, 417–423. doi: 10.1038/nclimate1726

Zagrodnik, J. P., McMurdie, L. A., and Houze, R. A. (2018). Stratiform precipitation processes in cyclones passing over a coastal mountain range. *J. Atmos. Sci.* 75, 983–1004. doi: 10.1175/JAS-D-17-0168.1

Zagrodnik, J. P., McMurdie, L. A., Houze, R. A., and Tanelli, S. (2019). Vertical structure and microphysical characteristics of frontal systems passing over a three-dimensional coastal mountain range. *J. Atmos. Sci.* 76, 1521–1546. doi: 10.1175/JAS-D-18-0279.1

Zhang, W., and Villarini, G. (2018). Uncovering the role of the East Asian jet stream and heterogeneities in atmospheric rivers affecting the western United States. *Proc. Natl. Acad. Sci. U. S. A.* 115, 891–96. doi: 10.1073/pnas.1717883115

Zhu, Y., and Newell, R. E. (1998). A proposed algorithm for moisture fluxes from atmospheric rivers. *Mthly. Weather Rev.* 126, 725–735. doi: 10.1175/1520-0493(1998)126<0725:APAFMF>2.0.CO;2

Conflict of Interest: The authors declare that the research was conducted in the absence of any commercial or financial relationships that could be construed as a potential conflict of interest.